

Charge-based quantum computing using single donors in semiconductors

L.C.L. Hollenberg*, A. S. Dzurak†, C. Wellard*, A. R. Hamilton†, D. J. Reilly†, G. J. Milburn‡ and R. G. Clark†

Centre for Quantum Computer Technology

** School of Physics, University of Melbourne, VIC 3010, Australia*

† Schools of Physics and Electrical Engineering, University of New South Wales, NSW 2052, Australia

‡ School of Physics, University of Queensland, QLD 4072, Australia

The construction of solid-state quantum computer architectures in which quantum bits (qubits) are encoded on the nuclear or electron spins associated with single atoms is now possible given recent advances in single-atom doping of semiconductors. Whilst these schemes have the promise of long coherence times they are not yet fully realizable due to the difficulty of single-spin detection. Here we present a two-atom charge qubit scheme for which fabrication and readout currently exist. The qubit consists of two dopant atoms ~ 50 nm apart in a semiconductor crystal, one of which is singly ionised. The lowest two energy states of the remaining electron form the logical states of the qubit. Surface electrodes control the qubit through applied voltage pulses and a single electron transistor operating near the quantum limit provides fast readout. Whilst the coherence time for charge-based qubits will be shorter than for their spin-based counterparts, the corresponding gate operation times will also be shorter, of order 50ps. We propose universal one- and two-qubit gate operations using this system and discuss the prospects for scale up.

In the search for an inherently scaleable quantum computer technology solid-state systems are of great interest. One of the most advanced proposals is based on superconducting qubits¹, where coherent control of qubits has been demonstrated, and decoherence times measured². Another promising scheme was proposed by Kane³, in which qubits are defined by long-lived nuclear spin states of buried phosphorus dopants in a silicon host crystal, and manipulated by external surface gates and RF magnetic fields. Recent advances in single dopant fabrication strategies⁴⁻⁶, together with demonstration of fast single electron transistor (SET) charge detection^{7,8}, bring the Kane architecture closer to reality. These important results notwithstanding, the demonstration of single spin readout remains as the major challenge for the Kane design. The charge qubit system introduced here is in many ways complementary to the Kane concept, yet it takes full advantage of the current conjunction of fast SET charge detection capability and single dopant fabrication processes, and requires no magnetic field.

The buried donor charge qubit is shown in Figure 1 for the case of P-dopants in Si. Although a number of candidate dopant-substrate systems are possible, we concentrate here on the case of Si:P. The lowest two states of the single valence electron localised by the double well formed by two donor P^+ atoms give rise to a natural identification of the quantum logic states. External control over the barrier height and potential off-set (or symmetry) is facilitated by B and S gates respectively, placed above the buried P-P⁺ system, as in Figure 1(b). With appropriate negative bias we can identify localised qubit states with high precision: $|0\rangle = |L\rangle$ and $|1\rangle = |R\rangle$, as shown in Figure 1(c). Finally, a SET facilitates initialization and readout of the qubit.

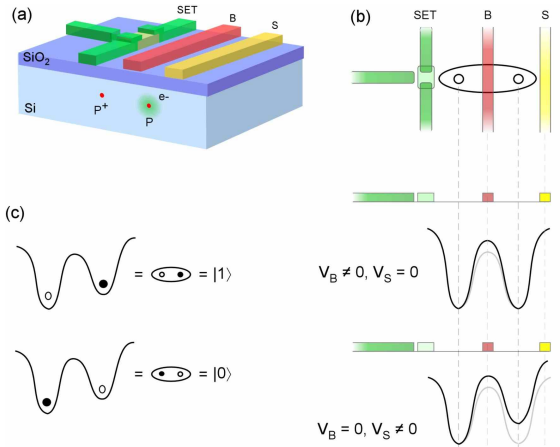


FIG 1. The buried charge qubit. (a) The solid-state charge qubit based on buried dopants D, forming a D-D⁺ system with one electron, shown explicitly for the case for Si:P. (b) The gated charge qubit showing barrier (B-gate) and symmetry (S-gate) control, together with a single electron transistor (SET) for charge-based readout. (c) One possible choice of logical states $|0\rangle$ and $|1\rangle$ – defined as shown in terms of left and right-localised states.

The charge qubit as defined is expected to decohere faster than the Kane nuclear spin qubit – however, as the analysis of qubit dynamics will show, the typical gate operation times of order 50ps are also commensurately faster than the μ s timescale⁹ of the spin qubit. In what follows we give estimates for the decoherence time associated with phonon interactions and gate fluctuations due to Johnston noise, and show that $\tau_{\text{op}} \ll \tau_{\phi}$ for these mechanisms. A more serious source of decoherence for all solid-state charge qubits is due to fluctuating background

charges. However, the measurements of Oosterkamp et al¹⁰ have shown that coherent quantum tunnelling of single electrons in coupled GaAs dots, which possess a similar vulnerability to background charge, can be maintained for timescales much longer than the single qubit operation time, and give a lower bound on τ_ϕ of 1ns. In comparison to the buried charge qubit the GaAs dots in those measurements were quite large – approximately $0.02\mu\text{m}^2$ in area with >30 electrons per dot. We conclude therefore that the quantum coherence time for the buried charge qubit will be at least sufficient to investigate small-scale devices in the first instance.

This paper is organised as follows. First, qubit dynamics are analysed to determine the fidelity of qubit states, and voltage gate control for single-qubit operations. The process of initialisation and SET readout are then outlined. Two possible qubit coupling schemes are described, and decoherence due to phonon mechanisms, gate fluctuations and charge traps is considered in the context of the typical gate operation times. Finally, fabrication of the charge qubit is described, and a possible scaled up N-qubit architecture is given.

The key to understanding single qubit gate operations is the effective Hamiltonian, H_Q , describing the dynamics of the P-P⁺ system in the presence of the S and B gates. In general, H_Q will be of the form:

$$H_Q = h_0(t) + h_x(t) \sigma_x + h_z(t) \sigma_z, \quad (1)$$

where the σ_i operate in the basis of qubit states. The qubit logical states are defined by application of reference gate configuration voltages (\bar{V}_B, \bar{V}_S), and are manipulated by fast-pulsed deviations ($\Delta V_B(t), \Delta V_S(t)$) from the reference configuration. Under these conditions, the time dependent coefficients in Eqn. 1 can then be written as:

$$\begin{aligned} h_0(t) &= \varepsilon_0 + \varepsilon_S \Delta V_S(t) + \varepsilon_B \Delta V_B(t) \\ h_x(t) &= X_0 + X_S \Delta V_S(t) + X_B \Delta V_B(t) \\ h_z(t) &= Z_0 + Z_S \Delta V_S(t) + Z_B \Delta V_B(t). \end{aligned} \quad (2)$$

The qubit dynamics are thus determined by the parameters ε_i , X_i and Z_i which depend explicitly on the donor separation, R , and the particular reference gate bias configuration (\bar{V}_B, \bar{V}_S). For the device shown in Figure 1 the spatial dependence of the potentials induced in the silicon substrate due to the gate voltages was modelled using TCAD¹¹. In all that follows we maintained a donor separation distance of $R \approx 27$ nm, and computed the effective Hamiltonian parameters by direct diagonalisation of the Hamiltonian in a basis of 12 molecular P-P⁺ states with parameters appropriate to donor electrons in Si: i.e. we use an effective Bohr radius of 3 nm and a single dopant electron ground state energy of -45 meV.

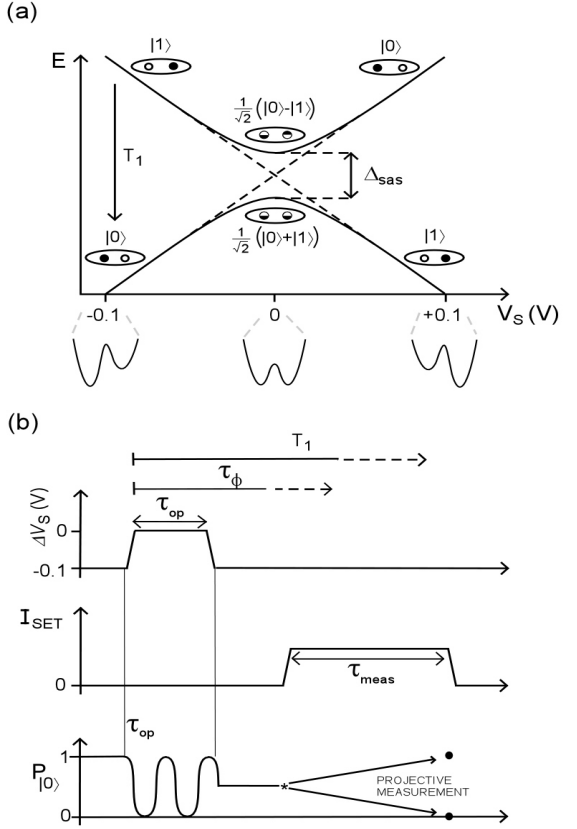


FIG 2. Qubit states and pulse timing. (a) Energy diagram illustrating the evolution of the eigenstates of the system as a function of applied S-gate bias, V_S , from left and right localised states ($|0\rangle = |L\rangle$ and $|1\rangle = |R\rangle$) through the mid-point (zero gate bias) where the eigenstates are equal superpositions of the localised states. (b) Pulse timing diagram and SET readout showing the relative timescales for gate operation (τ_{op}), SET readout (τ_{meas}), dephasing (τ_ϕ) and relaxation (T_1).

We have two choices for the basis of logical qubit states corresponding to the lowest two states being localised or delocalised. Since SET readout is carried out for localised states, we choose initially the configuration with non-zero S-gate bias, which serves to localize the electron into our qubit states as $|0\rangle = |L\rangle$ and $|1\rangle = |R\rangle$. Careful examination of the lowest two eigenstates of H_Q shows that for $\bar{V}_S \approx 0.1\text{V}$ the fidelity of qubit definition is optimal, with mixing of higher states less than 10^{-4} . We discuss later the alternative delocalised basis choice $|0\rangle = |A\rangle$ and $|1\rangle = |S\rangle$, for which decoherence effects will be less severe.

Once the qubit basis is determined by setting the reference gate configuration to $(\bar{V}_B, \bar{V}_S) = (0\text{V}, 0.1\text{V})$, the gate bias pulses ($\Delta V_B(t), \Delta V_S(t)$) required for qubit control can be read off from H_Q . For example, a $\pi/2$ rotation over 50ps requires gate bias pulse values of $\sim(0.40\text{V}, +0.10\text{V})$. Typically, single qubit rotations will require gate bias precision down to the mV level. The meaning of these

values of $(\Delta V_B(t), \Delta V_S(t))$ is illustrated in the adiabatic state diagram of Figure 2(a): the double well potential is adjusted to the symmetric position $V_S = 0$, while at the same time raising the barrier to slow the Rabi oscillations down to the O(50ps) time scales accessible to state-of-the-art pulse generation.

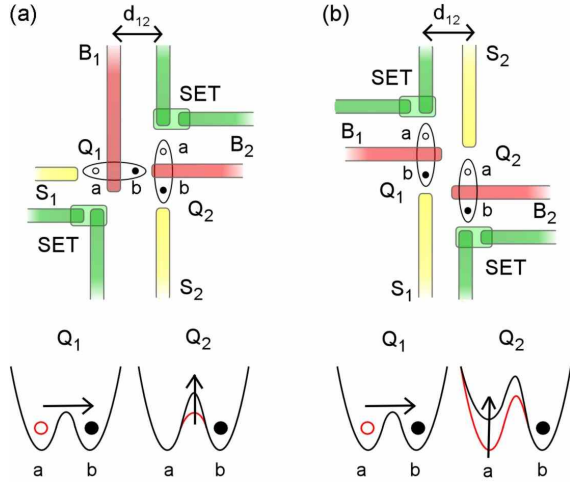


FIG 3. Qubit coupling schemes based on the Coulomb interaction. (a) A ‘‘CNOT’’ configuration where the control qubit Q_1 alters the effective barrier height as seen by the target qubit Q_2 , giving rise predominantly to an effective $\Gamma_{zx}\sigma_z^{(1)}\sigma_x^{(2)}$ interaction. (b) A ‘‘CPHASE’’ configuration corresponding to an effective $\Gamma_{zx}\sigma_z^{(1)}\sigma_z^{(2)}$ coupling.

Immediately after fabrication the qubit must be pre-initialised by removing one of the electrons from the P-P⁺ system to form the charge qubit. Using the S and B gates the electron in the right-hand donor well is ionised by a large S gate bias, at the same time the B-gate is raised to effectively isolate the electron in the left-hand well. After pre-initialisation, the SET conductance can be calibrated for the $|L\rangle$ and $|R\rangle$ states. Finally, initialisation of the charge qubit into the left state $|0\rangle$ is effected by simply biasing the S-gate and observing the SET conductance.

Prior to readout, the qubit is in a general state $|\psi\rangle = c_0|0\rangle + c_1|1\rangle$ resulting from a sequence of gate operations with the SET blockaded so that no current flows^{12,13}. As a result of projective measurement we wish to obtain $|0\rangle$ or $|1\rangle$ with probabilities $|c_0|^2$ and $|c_1|^2$ respectively. To perform such a projective measurement readout a voltage is applied to the SET bias gate tuning it to a conductance peak – the current flow through the device decoheres the charge qubit strongly, and causes a transition in time $\tau_\phi^{\text{SET}} \ll T_1$ to a statistical mixture of the localised eigenstates. Since the system has been calibrated in the pre-initialisation process, the SET will give a distinguishable reading, $I_{L,R}$, corresponding to the system having collapsed into the left or right state¹⁴. In Figure 2(b) the process of

readout following a sequence of qubit operations is illustrated schematically, showing the relative time scales.

In Figure 3 we present two distinct arrangements for qubit coupling, complete with gate structures and SET readout. For the case of the ‘‘CNOT’’ arrangement (Figure 3a), the horizontal qubit Q_1 acts on the effective barrier height of the vertical qubit Q_2 , and the coupling is primarily $\Gamma_{zx}\sigma_z^{(1)}\sigma_x^{(2)}$, while in the ‘‘CPHASE’’ scheme the effective coupling is $\Gamma_{zx}\sigma_z^{(1)}\sigma_z^{(2)}$. An in-depth investigation of the coupled qubit dynamics, controlled by such relatively complex gate structures, is beyond the scope of this paper, however, we have performed a preliminary semi-classical calculation to obtain an order of magnitude estimate. By moving a charge of 1.0 e between the a and b positions of Q_1 on Q_2 (shown in Figure 3, with a and b chosen to be 30-60 nm respectively from Q_2), we calculate a coupling strength of $\Gamma \approx 10^{-4} \rightarrow 10^{-5}\text{ meV}$. The corresponding coupled qubit operation times of $0.1 \rightarrow 1\text{ ns}$ are directly obtained from this estimate.

For the case of real quantum systems, coherence is unavoidably limited by environmental coupling. Successful operation of quantum devices is contingent on coherence times remaining longer than the time required for arbitrary rotations. In estimating the effect of the relevant decoherence mechanisms we follow similar treatments to those considered for superconducting Josephson devices. At an operating temperature of 100 mK dissipation from thermal phonons is negligible, owing to the small number of phonons with wavelengths able to couple to the qubit. A recent calculation of LA phonon induced decoherence on the P-P⁺ system¹⁵ concluded that for donor separations of 25 nm and greater, $\tau_\phi^{\text{phonon}}$ is of order μs , indicating that a large number of gate operations could be performed before phonons decohere the qubit.

An analysis of decoherence due to noise fluctuations on the S and B gates can be carried out using a Master equation approach¹⁶. While the qubit is in a quiescent state, the dominant off-diagonal (od) contribution to the density matrix is:

$$\rho_{od}(t) \approx \exp[-Z_S^2 \lambda_S t / 2\hbar^2],$$

where λ_S scales the fluctuations and is given by the Johnson formula: $\lambda_S = Rk_B T / \pi$. Using low temperature electronics at $T \sim 10\text{ K}$ and $R \sim 50\Omega$, we obtain:

$$\tau_\phi^{\text{Johnson}} \approx 2\pi\hbar^2 / Rk_B T Z_S^2 \sim 720\text{ ns}.$$

Finally, we consider 1/f noise from charge fluctuations in the surrounding environment, which is believed to be a serious limitation for all charge-based qubits¹⁷. In particular, individual charge traps can produce sudden and large changes in the noise signal at random times (random telegraph signals). To date coherence times of $\sim 1\text{ ns}$ have

been observed both in superconducting charge qubits¹⁸ and large semiconductor quantum dots¹⁰ providing a worst case lower bound on $\tau_\phi > 1\text{ns}$ for the buried charge qubit (given that single donor potentials represent the strongest confinement possible for a quantum dot). Although a serious issue, the use of high quality materials with low trap densities and refocusing pulse techniques may further extend the decoherence time. Furthermore, operation of the two-donor system in the delocalised basis should, in analogy to Josephson ‘phase’ qubits, lead to a significant suppression of the dephasing effects of charge noise¹⁹.

Realisation of the devices shown in Figures 1 and 3 requires an ability to dope a semiconductor at the single donor level with interdonor spacings in the range 20-100 nm. Due to the long range nature of the Coulomb coupling and the ability to tune the intra-qubit tunnelling rate using the B-gate, constraints on the donor spacings are significantly relaxed in comparison with previous spin-based schemes³.

Single atom doping of a semiconductor with the required positional accuracy has recently been demonstrated by two contrasting approaches. In the first, scanning-probe lithography of a hydrogenated silicon surface together with epitaxial Si overgrowth are used to construct a buried P array with precision $< 1\text{ nm}$ using atomic assembly^{4,5}. In the second, the donors are implanted through an array of nanoscale apertures and on-chip ion impact detectors are used to ensure that just one P ion passes through each aperture⁶. The positional accuracy of the second approach is limited by the straggle which occurs during implantation and will be comparable to the donor depth (10-20 nm). Both approaches, although currently developed for Si:P, can in principle be applied to other systems, such as GaAs:Si.

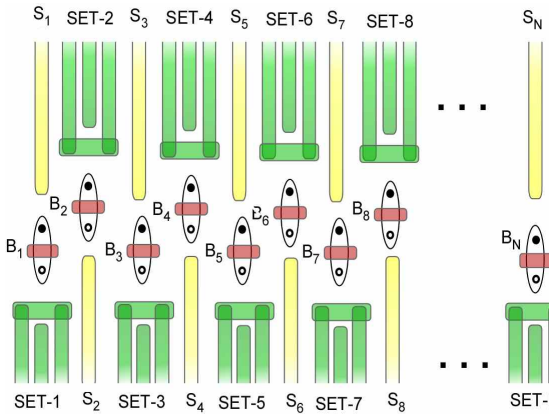


FIG 4. Schematic of a scaled-up architecture based on the staggered ‘CPHASE’ configuration.

Devices which incorporate buried donors, together with surface gates and SETs all registered to better than 20 nm, have recently been fabricated⁶. These devices incorporate two SETs which can be used to simultaneously monitor the

transfer of a single electron between two sites separated by $\sim 100\text{ nm}$. When combined with appropriate control and measurement electronics such devices allow gate voltage pulses on timescales $< 50\text{ ps}$ and can perform single-shot projective measurements of electron position on timescales of order $10\text{ ns}-1\mu\text{s}$ ^{20,21}. It is therefore anticipated that one-qubit experiments on such structures will be possible soon.

With single atom doping and SET readout schemes for Si:P now available it is expected that N-qubit architectures could be constructed in the near future. Figure 4 is a straightforward extension of the two-qubit CPHASE gate of Figure 3(b), where each qubit has an associated readout SET as well as the required S- and B-gates. The SETs would most conveniently be located on alternating sides of the one-dimensional array of qubits in order to localise the readout to the target qubit. Vertical via connections will be needed to make contact to the central B-gates, necessitating layered insulator and metal structures, although this is standard in modern VLSI circuits.

We have presented in some detail the concept of quantum computing based on buried-dopant charge qubits. Timescales for gate operations down to the limit of pulse generator technology have been shown to be entirely within the reach of current fabrication techniques developed for the Kane spin-based architecture, and are well within the estimates for decoherence due to phonons and gate fluctuations. The effect of environmental charge fluctuations can be gauged by the recent measurements of $\tau_\phi \sim 1\text{ ns}$ for electron tunnelling between coupled GaAs dots¹⁰, which can be considered as a lower bound in our case given that these structures effectively have many more degrees of freedom than a buried donor based qubit. Furthermore, 1/f noise due to interfacial charge traps acquired during the fabrication process can be minimised by considering buried charge qubits in an alternative system, such as GaAs:Si.

Finally, the coherence time may be increased significantly by defining the logical states in terms of delocalised symmetric and anti-symmetric states. Since the delocalised states have a very similar charge distribution they will be much less vulnerable to environmental charge fluctuations. This reduction in decoherence for de-localised logical states has been demonstrated for superconducting charge qubits¹⁹, extending the coherence time to 500ns.

This work was supported in part by the Australian Research Council, the Australian Government, the US National Security Agency, the Advanced Research and Development Activity and the US Army Research Office under contract number DAAD19-01-1-0653. The authors acknowledge discussions with C.I. Pakes, H.S. Goan and T.C. Ralph.

References

¹ A. Shnirman, G. Schoen and Z. Hermon, *Phys. Rev. Lett.* **79**, 2371 (1997).

² Y. Nakamura, Yu A. Pashkin and J.S. Tsai, *Nature* **398**, 786 (1999).

³ B.E. Kane, *Nature* **393**, 133 (1998).

⁴ J.L. O'Brien *et al.*, *Phys. Rev. B* **64**, 161401 (2001).

⁵ S.R. Schofield, N.J. Curson, M.Y. Simmons, L. Oberbeck, T. Hallam, F.J. Ruess and R.G. Clark, unpublished.

⁶ A.S. Dzurak *et al.*, unpublished.

⁷ R.J. Schoelkopf, P. Wahlgren, A.A. Kozhevnikov, P. Delsing and D.E. Prober, *Science* **280**, 1238 (1998).

⁸ A. Aassime, G. Johansson, G. Wendin, R.J. Schoelkopf and P. Delsing, *Phys. Rev. Lett.* **86**, 3376 (2001).

⁹ A. Fowler, C. Wellard and L.C.L. Hollenberg, *Phys. Rev. A* **67**, 012301 (2003).

¹⁰ T.H. Oosterkamp, T. Fujisawa, W.G. van der Wiel, K. Ishibashi, R.V. Hijman, S. Tarucha, L.P. Kouwenhoven, *Nature* **395**, 873 (1998).

¹¹ Technology Computer Aided Design (TCAD), Integrated Systems Engineering AG, Zurich.

¹² A.A. Clerk, S.M. Girvin, A.K. Nguyen and A.D. Stone, *Phys. Rev. Lett.* **89**, 176804 (2002).

¹³ M.H. Devoret and R.J. Schoelkopf, *Nature* **406**, 1039 (2000).

¹⁴ C.I. Pakes, V. Conrad, J.C. Ang, F. Green, A.S. Dzurak, L.C.L. Hollenberg, D.N. Jamieson and R.G. Clark, *Nanotechnology* **14**, 161 (2003).

¹⁵ S. Barrett and G.J. Milburn, cond-mat/0302238.

¹⁶ C. Wellard and L.C.L. Hollenberg, *J. Phys. D* **35**, 2499 (2002).

¹⁷ E. Paladino, L. Faoro, G. Falci, and R. Fazio, *Phys. Rev. Lett.* **88**, 228304 (2002).

¹⁸ J.S. Tsai, Y. Nakamura and Yu Pashkin, *Physica C* **367**, 191 (2002).

¹⁹ D. Vion *et al.*, *Science* **296**, 886 (2002).

²⁰ T.M. Buehler, D.J. Reilly, R. Brenner, A.R. Hamilton, A.S. Dzurak and R.G. Clark, *Appl. Phys. Lett.* **82**, 577 (2003).

²¹ T.M. Buehler, D.J. Reilly, R.P. Starrett, A.D. Greentree, A.R. Hamilton, A.S. Dzurak and R.G. Clark, cond-mat/0304384; T.M. Buehler, D.J. Reilly, R.P. Starrett, A.R. Hamilton, A.S. Dzurak and R.G. Clark, cond-mat/0304385.